JOURNAL OF THE ROYAL SOCIETY Interface

Design of biomimetic fibrillar interfaces: 1. Making contact

N. J. Glassmaker, A. Jagota, C.-Y. Hui and J. Kim

J. R. Soc. Interface 2004 **1**, 23-33
doi: 10.1098/rsif.2004.0004

THE ROYAL SOCIETY

J. R. Soc. Interface (2004) 1, 23–33
DOI: 10.1098/rsif.2004.0004

Design of biomimetic fibrillar interfaces: 1. Making contact

N. J. Glassmaker[1,†], A. Jagota[2,‡], C.-Y. Hui[1] and J. Kim[2]

[1] *Department of Theoretical and Applied Mechanics, Cornell University, 212 Kimball Hall, Ithaca, NY 14853, USA*
[2] *DuPont Central Research & Development, Experimental Station, E356/261, Wilmington, DE 19880, USA*

This paper explores the contact behaviour of simple fibrillar interfaces designed to mimic natural contact surfaces in lizards and insects. A simple model of bending and buckling of fibrils shows that such a structure can enhance compliance considerably. Contact experiments on poly(dimethylsiloxane) (PDMS) fibrils confirm the model predictions. Although buckling increases compliance, it also reduces adhesion by breaking contact between fibril ends and the substrate. Also, while slender fibrils are preferred from the viewpoint of enhanced compliance, their lateral collapse under the action of surface forces limits the aspect ratio achievable. We have developed a quantitative model to understand this phenomenon, which is shown to be in good agreement with experiments.

Keywords: fibril; fibrillar adhesion; biological mimic; buckling; dry adhesion; contact mechanics

1. INTRODUCTION

Many animals achieve controlled contact, tribology and adhesion via designed surfaces (see Autumn *et al.* 2000, 2002; Artz *et al.* 2003; Scherge & Gorb 2001; Rischick *et al.* 1996). In many cases, nature has evolved variations of fibrillar surfaces, for example in lizards such as geckos (Autumn *et al.* 2000) and skinks (Rischick *et al.* 1996), and in insects (Scherge & Gorb 2001). Independent evolution of these structures, employing different but related sets of materials, suggests that their geometry has some universal benefits. Consequently, the mimicry of these structures using synthetic materials has excited considerable recent interest, with hopes that the mimic structures will have the same properties as those found in biology.

The distinctiveness of the solutions that biology has provided consists, for the most part, in their ability to make contact with a variety of surfaces while using materials considerably stiffer than those used in pressure sensitive adhesives. Several other unique features of such 'setal' adhesion have been noted in the literature, including their self-cleaning ability, directional adhesion and controlled release mechanisms (see Autumn *et al.* 2000; Artz *et al.* 2003). Consistent with the non-material specific nature of setal contact and adhesion, it has been shown that fibrillar adhesion relies either on ubiquitous van der Waals interactions (Autumn *et al.* 2000, 2002) or on capillary forces (Scherge & Gorb 2001), or both. That synthetic mimics can enhance adhesive properties by use of a fibrillar architecture has recently been demonstrated using micro-fabrication to pattern a polyimide film (Geim *et al.* 2003). The companion paper to this one (Hui *et al.* 2004) also presents experimental results showing enhanced adhesion for synthetic poly(dimethylsiloxane) (PDMS) fibrillar surfaces, as does recent work by Peressadko & Gorb (2004) for another elastomeric material.

Within the common theme of a fibrillar design, different animals have evolved separate variations. These include geometrical parameters such as fibril dimensions and density, and details such as hierarchical levels (if any) and flattened tip structures (spatulae). It is clear that the architecture needs to be designed and optimized carefully for the structure to deliver the desired contact and adhesive performance. The fibril design question is of interest both to understand the natural structures and to provide guidance and design principles for their bio-mimicry. There are few quantitative studies that address this question, which is the main topic of this and a companion paper (Hui *et al.* 2004).

In approaching the question of the physics and mechanics of contact and adhesion of fibrillar interfaces it is useful to group the issues into two broad categories, each addressing one of the following questions: (a) How does a fibrillar interface allow for controlled and intimate contact in the presence of rough and uncontrolled opposing surfaces? (b) How does a fibrillar interface behave when separated from a substrate; in particular, what is its effect on adhesion enhancement? Specific issues related to these questions have been outlined by Jagota & Bennison (2002), Arzt *et al.* (2003) and Persson (2003*a*), with the first work drawing upon

† Author for correspondence (njg22@cornell.edu).
‡ Present address: Department of Chemical Engineering, Lehigh University, 111 Research Drive, Iacocca Hall, Bethlehem, PA 18015, USA.

Received 6 February 2004
Accepted 3 June 2004
Published online 7 July 2004

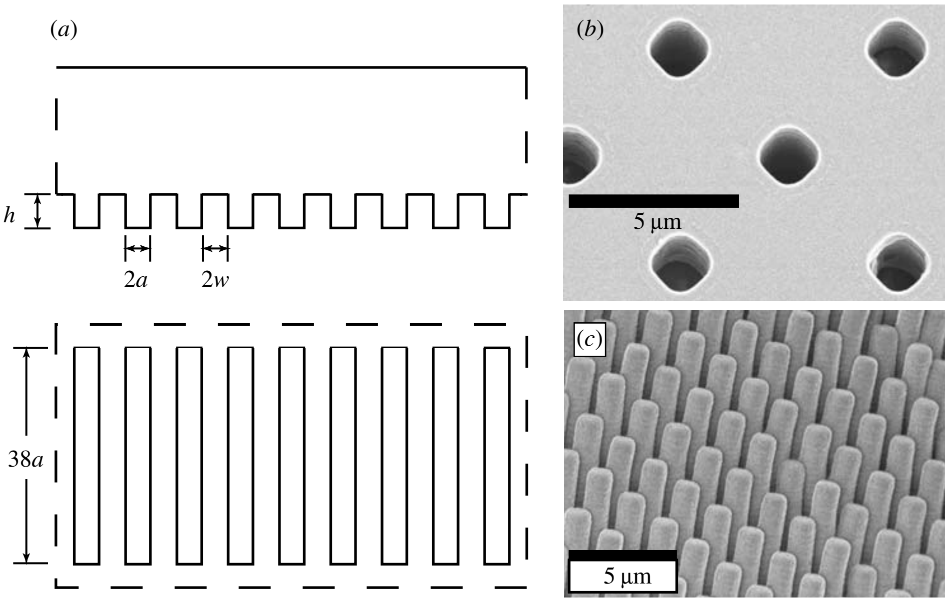

Figure 1. (*a*) Schematic (not to scale) of geometry I: plate-like fibrils. Dashed lines indicate symmetry planes where the pattern repeats. (*b*), (*c*) Scanning electron microscope (SEM) images of geometry II: post-like fibrils: (*b*) silicon master with ion-etched holes used to mould PDMS; (c) resulting fibrillar PDMS structure.

a detailed theory of the mechanics of micro-contact printing (see Hui *et al.* 2002; Sharp *et al.* 2004). It has been suggested by Arzt *et al.* (2003) that the reduction of setal diameter with increased animal mass is directly related to the increased total adhesive force based on an application of the Johnson–Kendall–Roberts (JKR) theory of adhesive contact (see Johnson *et al.* 1971). Jagota & Bennison (2002) and Persson (2003*a*) have argued that a fibrillar structure provides compliance and enhances adhesion primarily by loss of energy stored in fibrils. However, these two arguments rely on basically different measures of adhesive performance and are hence somewhat incompatible.

In this and the companion paper (Hui *et al.* 2004), we develop a quantitative theory for contact and adhesion of fibrillar interfaces that, among other things, attempts to resolve this incompatibility. Here, in the first part, we consider how materials and geometrical parameters of a fibrillar structure control surface contact (question (a) above). We discuss lateral flexibility of fibrils and micro-buckling as deformation modes that significantly reduce the interfacial stiffness; our predicted results compare well with experiments on a model fibrillar interface. (Note that by ‘micro-buckling’ we mean buckling of the fibrillar structures, as opposed to buckling at a larger scale in the overall structure.) Lateral collapse, i.e. bonding of neighbouring fibrils, limits the aspect ratios achievable; we quantify this notion and show our results to be predictive. We suggest that hierarchical structures observed in nature may result as a way of defeating this constraint. The companion paper develops the second part of our study on adhesion enhancement by fibrils (question (b) above). We restrict our attention here to the simplest fibrillar structures for the sake of comparison with well-controlled experimental materials. For example, in this paper, we do not address the question of the advantages provided by thin plate-like spatular structures that terminate most natural fibrils, which clearly play an important role in adhesion to rough surfaces (Persson 2003*b*).

2. EXPERIMENTAL DETAILS

To motivate our theoretical calculations, we briefly describe in this section the geometry of the experimental samples under consideration, the methods used to fabricate them and the types of contact mechanics experiments performed on them. Results of experimental measurements will be presented after the theoretical section, to facilitate understanding and comparison between theoretical predictions and experimental data.

Model experimental fibrillar structures were fabricated by the moulding of an elastomer using negative-image masters patterned by photolithography. For the elastomer, we used poly(dimethylsiloxane) (PDMS) (Sylgard 184®, Dow Chemicals) in a ratio of 10:1 (rubber base:cure). This silicone mixture was outgassed under vacuum for 30 minutes before applying to the master and was cured at a temperature of 50 °C for 48 hours on the master. In one case (geometry I), masters were fabricated with four isolated regions ($5\times5\,\mathrm{mm}^2$ each) containing rectangular relief patterns of differing scales. The fibril width $2a$ and spacing $2w$ were such that $2a=2w=5$, 10, 20 or 50 µm. The structures were 19 times as long as they were wide and their height h was dictated by the thickness of the photoresist layer (~30 µm), see figure 1*a*. These samples will be referred to as ‘plate-like’ fibrillar surfaces.

Other masters were fabricated by etching 10 µm deep cylindrical holes with 1 µm cross-sectional dimension into Si. Holes were etched by first patterning 4-inch Si wafers with deep-ultraviolet (DUV) photolithography and then using the photoresist pattern as a mask for deep reactive ion etching of the Si wafer. The corresponding moulded PDMS structures for these

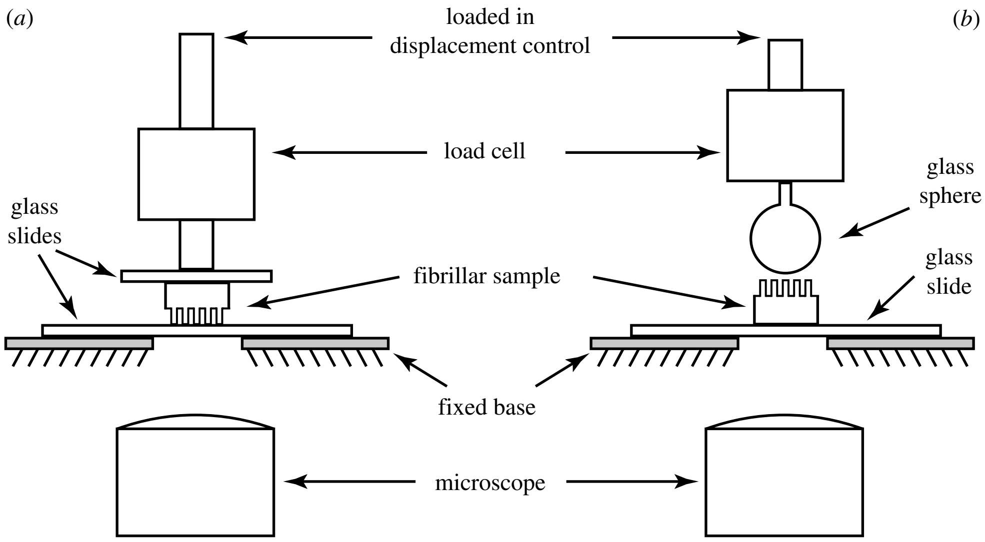

Figure 2. Schematics of the set-ups for contact experiments: (*a*) fibrils contacting the flat glass substrate; (*b*) fibrils contacting the spherical glass indenter.

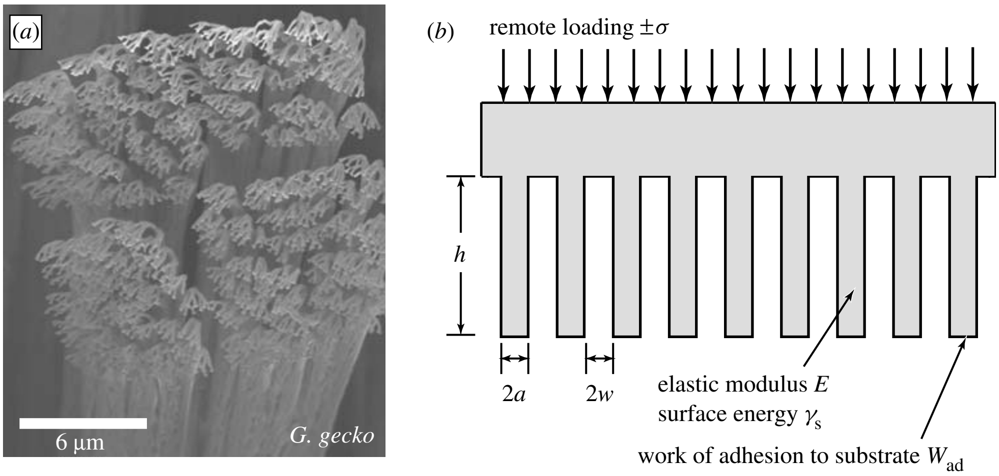

Figure 3. (*a*) Hierarchical fibrillar structure in *G. gecko*, terminating in thin spatulae (courtesy N. Rizzo, DuPont). (*b*) Schematic of the idealized fibrillar architecture considered here.

masters are cylindrical fibrils (geometry II). See figures 1*b* and 1*c*. These samples will be referred to as 'post-like' fibrillar surfaces.

Both types of samples underwent contact experiments, where the specimen was placed on a glass slide and viewed with an inverted microscope. Fibrils either contacted the glass slide or pointed upwards and away from the microscope objective. The sample was loaded under precise displacement control, with concurrent force measurement via a load cell and deformation visualization through the microscope. Loading was applied either via a flat piece of glass or with a spherical glass indenter (figure 2). Load–displacement curves were acquired at various strain rates with the visual information captured by a video recorder.

3. THEORETICAL RESULTS

Figure 3*a* shows the fibrillar structure of setae in *Gekko gecko*. The hierarchical and bent nature of the fibrils is evident. While a hierarchical structure is common, it is not universal. For example, in the genus *Anolis* one often finds a single-level fibrillar structure. In this and the companion paper (Hui *et al.* 2004), for the sake of concreteness and to develop a comprehensive set of results, we consider a simple idealized fibrillar structure consisting of a single-level array of micro-beams protruding from a substrate or backing (figure 3*b*). Consideration of this simplified structure allows us to be precise in analysing different modes of deformation, while maintaining the essential elements of the natural structures. In addition, the structure shown in figure 3*b* corresponds directly to the simplest fibrillar mimics that we and others have fabricated (see the previous section and Geim *et al.* 2003). It consists of beams with a given cross section, characterized by Young's modulus E, moment of inertia I, length h and cross-sectional dimension $2a$. The beams are separated by a characteristic distance $2w$ and cover a contact area fraction f. To illustrate some of the theoretical results

Table 1. Two sets of material properties representing typical soft and stiff polymeric materials.

Parameter	Soft material	Stiff material
Young's modulus E	1 MPa	10^3 MPa
Work of adhesion $W_{\mathrm{ad}} = 2\gamma_{\mathrm{s}}$	$100\,\mathrm{mJ\,m^{-2}}$	$100\,\mathrm{mJ\,m^{-2}}$

we will use two sets of typical material properties as shown in Table 1, which are representative of a soft elastomer and a stiffer glassy polymer material. For identical materials in contact, the work of adhesion is $2\gamma_{\mathrm{s}}$, where γ_{s} is the surface energy.

3.1. Contact flexibility of a fibrillar interface

Single fibril stress–strain analysis. As one lowers the stiffness of a material, it is able to conform to surfaces with increasing roughness, for the same given applied load (Jagota & Bennison 2002; Hui *et al.* 2002). Indeed, this is well known to be part of the basic mechanism by which pressure-sensitive adhesives work. There are some disadvantages associated with the use of a low modulus material, however. Most notably, for a flat surface to conform to a rough mating surface, very compliant material properties are required. As a result, the material tends to creep and foul by particulate contamination (Jagota & Bennison 2002).

By contrast, a fibrillar interface can deliver a compliant response while still employing stiff materials because of bending and micro-buckling of fibrils. The synthetic fibrillar surfaces that are simplest to fabricate have fibrils oriented normal to their backing and hence to the contacting surface. For such a structure, micro-buckling makes the structure very compliant compared to the pre-buckled state. Based on classical Euler buckling (Hui *et al.* 2002; Timoshenko & Gere 1961), for a uniform applied stress, micro-buckling occurs when the force normal to the fibril exceeds a critical value, F_{cr}, given by

$$F_{\mathrm{cr}} = b_{\mathrm{c}} \frac{\pi^2 E^* I}{h^2}, \tag{3.1}$$

where $E^* = E/(1-\nu^2)$ is the plane strain fibril modulus, ν is Poisson's ratio and b_{c} is a factor of the order of unity that depends on boundary conditions. For example, $b_{\mathrm{c}} \sim 2$ for pinned–clamped micro-beams. Note that equation (3.1) is only valid for fibrils that are long in one of the directions normal to their height, e.g. the plate-like fibrils shown schematically in figure 1*a*. We verified experimentally that the buckling predicted in compression does occur in plate-like fibrillar structures (Sharp *et al.* 2004). Moreover, the buckling load on loading was found to be different from that seen on unloading; this has been explained and modelled by modifying classical Euler buckling to account for adhesion between the fibril ends and a substrate (Glassmaker 2004).

In the current analysis, we consider fibrils that extend away from a backing at an angle other than $\pi/2$ (see figure 4*a*). This analysis will allow one to determine how compliance is increased both by bending and axial deformation. Assuming the contact force F is aligned normal to the backing, its components along and tangential to the direction of the fibril, $F\cos\theta$ and $F\sin\theta$, give rise to bending and compressive deformations, δ_{b} and δ_{c}, respectively. Using standard results for compliance of a beam and rod (Crandall *et al.* 1978),

$$\delta_{\mathrm{b}} = \frac{F\cos\theta h^3}{3EI}, \quad \delta_{\mathrm{c}} = \frac{F\sin\theta h}{AE}, \tag{3.2}$$

where A and I are the cross-sectional area and moment of inertia of the fibril, respectively. The net displacement normal to the backing is given by

$$\delta_{\mathrm{n}} = \delta_{\mathrm{c}}\sin\theta + \delta_{\mathrm{b}}\cos\theta = \frac{F\cos^2\theta h^3}{3EI} + \frac{F\sin^2\theta h}{AE}. \tag{3.3}$$

The remote applied stress (normal to the substrate) is given by $\sigma = fFA^{-1}\sin\theta$, where f is the area fraction of the top of the fibrillar surface that makes contact, while strain in the fibrillar region is $\varepsilon_{\mathrm{n}} = \delta_{\mathrm{n}}/(h\sin\theta)$. The contact area fraction f defined here is more general than the area fraction ρ used in the companion paper (Hui *et al.* 2004), since we allow fibrils to be attached to the backing at an angle θ other than $\pi/2$. To be specific, $f = NA/\sin\theta$, where N is the number of fibrils per unit area of the backing. Note that $\rho = NA$, so that $f = \rho$ when $\theta = \pi/2$. Substituting these definitions into (3.3) yields a stress–strain relationship for the fibrillar mat. In addition, applying the buckling condition (3.1) gives a critical compressive strain for buckling, $\varepsilon_{\mathrm{cr}}$. Together, these are

$$\left.\begin{aligned} \frac{\sigma}{E} &= \frac{f}{1+(Ah^2/3I)\cot^2\theta}\varepsilon_{\mathrm{n}}, \\ \varepsilon_{\mathrm{cr}} &= -\frac{b_{\mathrm{c}}\pi^2}{3(Ah^2/3I)}\left(1+\frac{Ah^2}{3I}\cot^2\theta\right). \end{aligned}\right\} \tag{3.4}$$

For fibrils having a rectangular cross section with sides of length $2a$ and b, $I = 2ba^3/3$ and $A = 2ab$,

$$\left.\begin{aligned} \frac{\sigma}{E} &= \frac{f}{1+(h^2/a^2)\cot^2\theta}\varepsilon_{\mathrm{n}}, \\ \varepsilon_{\mathrm{cr}} &= -\frac{b_{\mathrm{c}}\pi^2 a^2}{3h^2}\left(1+\frac{h^2}{a^2}\cot^2\theta\right). \end{aligned}\right\} \tag{3.5}$$

If $b \gg a$, which is a requirement for the second expression in each of (3.4) and (3.5) to hold, deformation along the long direction can be assumed to be constrained by the substrate. Then, one can assume plane strain deformation by replacing E with E^* and setting $b = 1$ in equations (3.4) and (3.5).

Figure 4*b* plots this case of equation (3.5) for $h/a = 12$, $f = 0.5$ and $b_{\mathrm{c}} = 2$, which are representative parameters for the 5 µm plate-like fibrils (narrowest case) used in our experiments. For $\theta = 90°$, the response is the stiffest in tension and compression, being governed by extensional elasticity. With departure of angle θ from $\pi/2$, the structure becomes increasingly compliant as bending deformation becomes dominant. In tension the maximum load is limited by decohesion mechanics, which have been analysed in the companion paper (Hui *et al.* 2004). Here, for the sake of simple illustration, it has been set by fixing an (arbitrary) maximum strain.

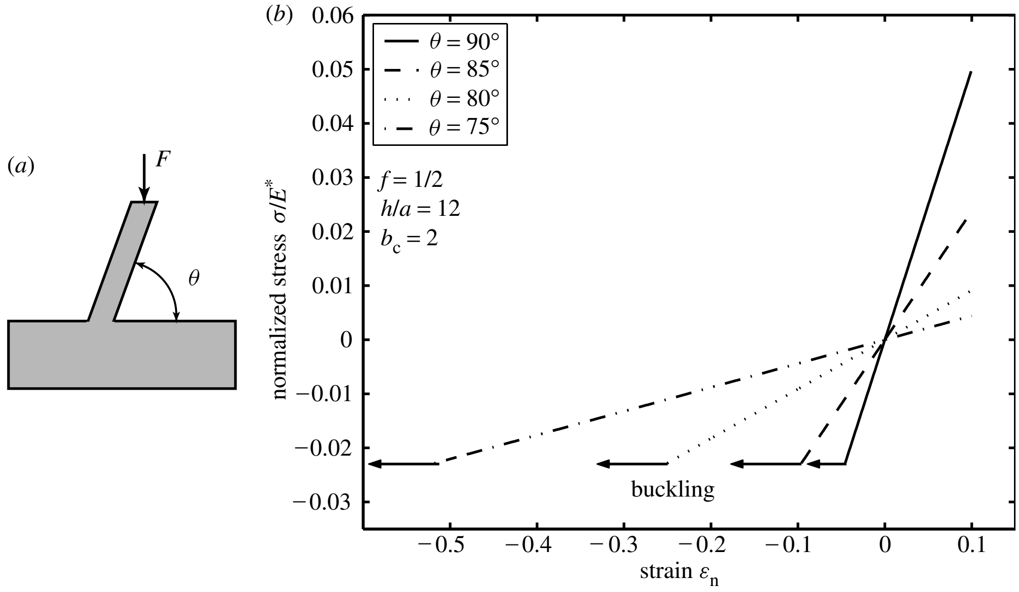

Figure 4. (*a*) Schematic of a fibril oriented at an angle θ relative to its backing. (*b*) Plot of theoretically calculated stress versus strain for fibrillar interfaces with various orientations relative to their backings.

In compression, micro-fibrils buckle at a critical stress. This results in a mechanical response that resembles plastic yielding, in the sense that at the critical stress there is no incremental load-carrying capacity. As a potential advantage, this offers much reduced compliance. However, the exploitation of buckling as a softening mechanism has an attendant difficulty because it may result in decohesion of fibril ends.

Buckling stress analysis for many fibrils indented by a rigid sphere. We analyse the spherical indentation experiment shown in figure 2*b* using the JKR theory of elastic contact (see Johnson *et al.* 1971). Although this theory is meant for smooth (non-fibrillar) interfaces, it is applied here with the understanding that it will be valid if the contact region is considerably larger than fibril dimensions and that the extracted modulus and adhesion should be interpreted as effective quantities. This is equivalent to treating the patterned PDMS as an effective flat elastic half-space with a different modulus E^* and work of adhesion W_{ad} than an actual flat half-space of PDMS.

Figure 5 shows typical force–deflection data from spherical indentation of a flat PDMS sample; indentation data from fibrillar samples are similar. The elastic modulus is obtained by noting that, for sufficiently large displacement δ (i.e. when the force is non-tensile so that adhesion plays a negligible role in the deformation), the load–displacement relation should be well approximated by the Hertz contact theory (see Johnson 1985), which states that

$$F = 4E^*\sqrt{R}\,\delta^{3/2}/3, \tag{3.6}$$

where E^* is defined as above, $v \approx 1/2$ is Poisson's ratio of PDMS and R is the radius of the sphere. Note that the contact mechanics convention that positive forces are compressive is used in (3.6) and in the rest of this section. The effective work of adhesion is related to the magnitude of the maximum tensile load $-F_{\max}$ by

$$W_{\mathrm{ad}} = \frac{-2F_{\max}}{3\pi R}. \tag{3.7}$$

The theoretical buckling load for an individual plate-like fibril is given by equation (1), i.e.

$$P_{\mathrm{c}} \approx \frac{1.36\pi^2 E^* a^3}{8h^2} \tag{3.8}$$

(Hui *et al.* 2002). Thus, once E^* is found by fitting equation (3.6) to the load–displacement data at sufficiently large displacements, the theoretical buckling load is determined.

For a rigid sphere indenting an elastic half-space, the JKR pressure distribution $p(r)$ within the contact region, at a distance r from the centre of contact (Johnson *et al.* 1971), is

$$p(r) = p_0\left(1-\left(\frac{r}{C}\right)^2\right)^{1/2} + p_0'\left(1-\left(\frac{r}{C}\right)^2\right)^{-1/2}, \quad r < C, \tag{3.9}$$

where C is the contact radius and

$$p_0 = \frac{2CE^*}{\pi R} \quad \text{and} \quad p_0' = -\sqrt{\frac{2E^* W_{\mathrm{ad}}}{\pi C}}. \tag{3.10}$$

Note that it is sufficient to treat the glass sphere as rigid, since the elastic modulus of glass is five orders of magnitude greater than that of PDMS.

Given the estimates from (3.6) and (3.7) for E^* and W_{ad}, the JKR pressure distribution of equation (3.9) is determined. It is expected (and observed experimentally) that buckling will first occur at $r = 0$, where the contact pressure is maximum, i.e.

$$p_{\max} = p(0) = \frac{2CE^*}{\pi R} - \sqrt{\frac{2E^* W_{\mathrm{ad}}}{\pi C}}. \tag{3.11}$$

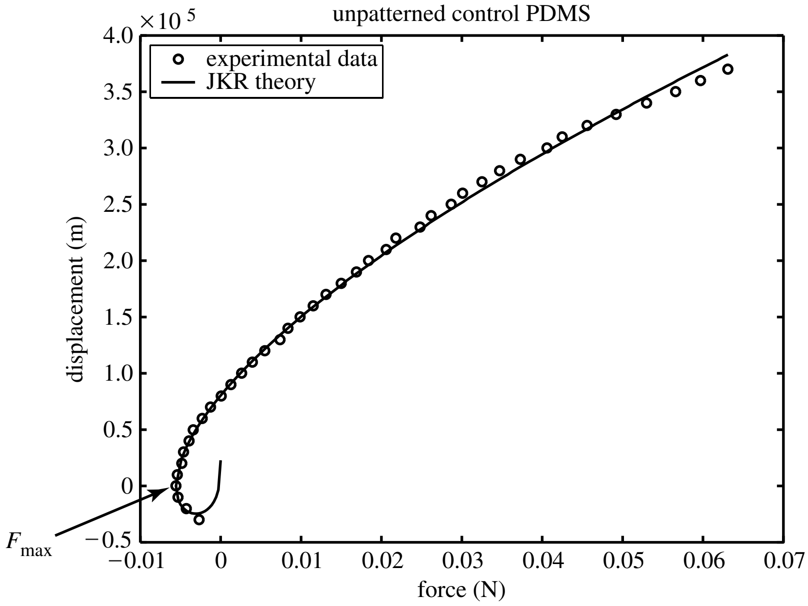

Figure 5. Load–displacement data for spherical indentation of PDMS including a fit to the JKR theory. (These data are from the part of the experiment when the sphere is pulled out of contact with the PDMS.)

Thus, an estimate for the experimental buckling load is

$$P_{\exp} = (2a + 2w)p_{\max}, \tag{3.12}$$

where the value of $p_{\max}$ corresponds to the contact radius C where buckling is first observed.

3.2. Lateral collapse

From the view point of enhanced energy dissipation (i.e. enhanced adhesion) and increased interfacial compliance, slender fibrillar structures with large aspect ratio are preferred (see Hui *et al.* 2004 and the previous section). However, the ability to make slender fibrils of sub-micrometre cross-sectional dimensions is limited by their tendency to collapse laterally under the influence of surface forces. Lateral collapse has also been noted as a mechanism that limits the adhesive performance of mimics (see Geim *et al.* 2003). We have previously established a condition for lateral collapse of plate-like fibrils (see Hui *et al.* 2002). To be specific, lateral collapse occurs when the separation $2w$ between fibrils is small enough so that

$$\frac{h}{2a}\left[\frac{4\gamma_s}{3E^*a}\right]^{1/4} > \sqrt{w/a}\,, \tag{3.13}$$

where $\gamma_s = W_{ad}/2$ is the surface energy. For our plate-like specimens, those with $2a = 10\,\mu m$ do not collapse laterally, while the $5\,\mu m$ fibrils do, in complete agreement with the prediction (3.13) (Sharp *et al.* 2004). Note that (3.13) is derived for fibrils with rectangular cross sections, where the entire lateral surface can be in contact. For fibrils with non-rectangular cross sections, e.g. those with circular cross sections (geometry II in figure 1*c*), the condition for lateral collapse is somewhat altered. In such cases, the contact radius can be much smaller than the radius of the cylinder and the material near the contact region is subject to elastic deformation that does not occur for rectangular cross sections.

Consider the case where the fibrils are long circular rods. When two such identical rods are placed in closed proximity, the surfaces will cause the rods to jump into contact and adhere. The equilibrium contact width $c_0 = 2r_c$ of two identical circular cylinders with radius R subject to *no external force* (no end constraints) can be determined using the JKR theory (Hui *et al.* 2000),

$$r_c = \left(\frac{32R^2\gamma_s}{\pi\ E*}\right)^{1/3}. \tag{3.14}$$

Due to deformation near the contact region, there is an accompanying stored elastic energy in the fibrils, U_c. The contact radius is established by the equilibrium condition

$$\frac{\partial U_c}{\partial r_c} = 4\gamma_s. \tag{3.15}$$

Using (3.14) in (3.15), integrating and restricting to the case of two identical cylinders gives the result

$$\frac{U_c}{ER^2} = \frac{\pi}{32(1-\nu^2)}\left(\frac{r_c}{R}\right)^4. \tag{3.16}$$

Figure 6 compares this analytical result with results obtained by numerical simulations using finite-element computations and shows excellent agreement over a broad range of contact radius.

Now we amend this result to model lateral collapse by including the constraint that at one end the beams are separated by a distance $2w$. Let the length of the non-contact portion of two laterally collapsed beams be denoted by L. The strain energy U_b associated with bending can be computed using elementary beam theory (see Crandall *et al.* 1978), i.e.

$$U_b = 12EIw^2/L^3. \tag{3.17}$$

The length of the non-contact region can be determined by an energy balance. Suppose the straight edge

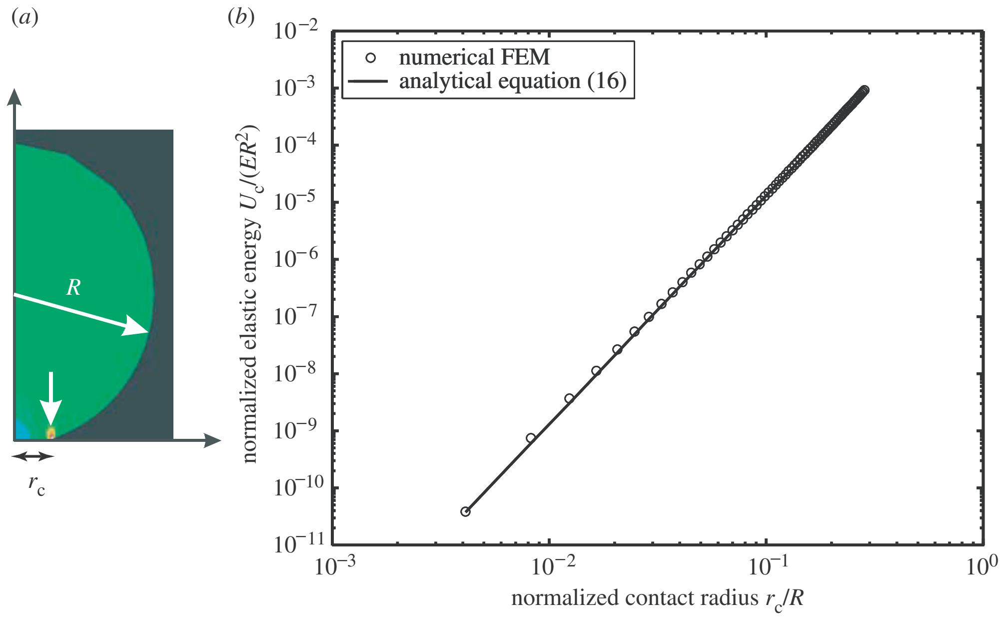

Figure 6. Relationship between stored elastic energy in two elastic cylinders contacting under the influence of surface forces. The cylinders are long in the direction parallel to their axes.

separating the contact and the non-contact regions is advanced by dL. The resulting decrease in strain energy is

$$-\frac{\mathrm{d}U_\mathrm{b}}{\mathrm{d}L} = \frac{36EIw^2}{L^4}. \tag{3.18}$$

Under equilibrium conditions, this decrease in strain energy is equal to the energy required to separate the two surfaces, which is $2\gamma_\mathrm{s}c_0\,\mathrm{d}L - U_\mathrm{c}\,\mathrm{d}L$. The length of the non-contact zone is determined by equating these two energies, i.e.

$$36EIw^2\,\mathrm{d}L/L^4 = (2\gamma_\mathrm{s}c_0 - U_\mathrm{c})\,\mathrm{d}L, \tag{3.19}$$

which results in

$$L = \left(\frac{36EIw^2}{2\gamma_\mathrm{s}c_0 - U_\mathrm{c}}\right)^{1/4}, \tag{3.20}$$

where $c_0 = 2r_\mathrm{c}$ is given by (3.14), U_c is given by (3.16) and $I = \pi R^4/4$.

The height of the fibril, h, must be less than L given by (3.20) in order for it not to collapse laterally, that is, lateral stability requires

$$\left(\frac{36EIw^2}{2\gamma_\mathrm{s}c_0 - U_\mathrm{c}}\right)^{1/4} > h. \tag{3.21}$$

Specifically, for rectangular and circular cylinders,

$$\left.\begin{aligned} \left(\frac{12Ea^3w^2}{\gamma_\mathrm{s}}\right)^{1/4} &> h, \quad \text{rectangle,} \\ \left(\frac{\pi^4E^*a}{2^{11}\gamma_\mathrm{s}}\right)^{1/12}\left(\frac{12Ea^3w^2}{\gamma_\mathrm{s}}\right)^{1/4} &> h, \quad \text{circle.} \end{aligned}\right\} \tag{3.22}$$

In (3.22), the first result is for a rectangular cross section with sides of length $2a$ and $2b$, contacting along the side of length $2b$. Note that the length of the contacting side, $2b$, does not affect when lateral collapse will occur, and that (3.22) is identical with (3.13) when $b \gg a$, so that E can be replaced with E^*. The second result is for a circular cross section with diameter $2a$. From (3.22), we see that the ratio of critical length for circular and rectangular fibrils with the same cross-sectional dimension is

$$\frac{h_\mathrm{c}}{h_\mathrm{r}} = \left(\frac{\pi^4E^*a}{2^{11}\gamma_\mathrm{s}}\right)^{1/12}. \tag{3.23}$$

For the soft material of Table 1 and a 1 μm fibril, this is about 0.996, while for the stiff material it is 1.77. That is, for the stiffer material, there is considerable advantage for avoiding lateral collapse in choosing a circular cross section over a rectangular one.

Equation (3.14), which applies specifically to fibrils with a circular cross section, can be readily extended to those with convex cross sections bounded by smooth curves. Let $f(x) = R\phi(x/R)$ denote the local shape of the bounding curve before contact. Then, using the results of Muskhelishvili (1951), the equilibrium contact length c_0 is determined by solving the equation

$$F(c_0/R) = 4\pi\sqrt{\gamma_\mathrm{s}/E^*c_0}\,, \tag{3.24}$$

where

$$F(c_0/R) = \int_{-1}^{1}\sqrt{\frac{1+t}{1-t}}\,f'\left(\frac{c_0t}{R}\right)\,\mathrm{d}t \tag{3.25}$$

and R is the local radius of curvature of the cross section of the fibril. For example, for a circular cylinder with radius R, $f(x) = x^2/R$.

4. EXPERIMENTAL RESULTS AND DISCUSSION

4.1. Spherical indentation

Spherical indentation (figure 2*b*) allows one to extract an effective modulus and an effective work of adhesion.

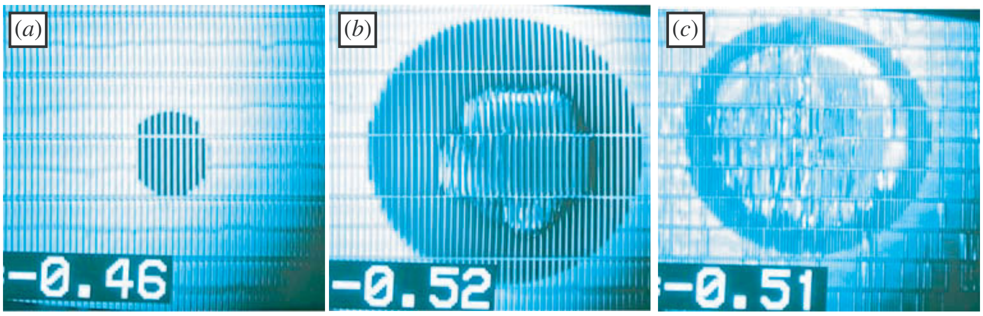

Figure 7. Three micrographs of indentation of a plate-like fibrillar interface ($2a = 10\,\mu m$, bottom view) with increasing applied load. (*a*) The contact region is nearly circular and, initially, all fibrils remain vertical and attached to the indenting sphere. (*b*) At a critical load, fibrils in a central region buckle. (*c*) The buckled region grows with increasing load and is surrounded by an annular region of contacting and upright fibrils. The fact that buckled fibrils lose contact with the indenter (true in this case, but perhaps not always) has detrimental consequences for adhesion, as presented later. The numbers on the pictures represent voltage readings from the load cell.

It can also be viewed as a simple instance of contact against an uneven surface, albeit one with 'roughness' on a length scale much greater than the fibril dimensions. The following results are for indentation by a rigid sphere (glass, radius of 4.01 mm). The PDMS specimens had plate-like fibrils (geometry I in figure 1*a*) with $h = 30\,\mu m$ and $2a = 50$, 20, 10 or $5\,\mu m$; a flat control PDMS specimen was subjected to identical experiments for comparison. The backing film behind the fibrils was approximately 2 mm thick. Experiments were performed at two rates, $1\,\mu m\,s^{-1}$ and $10\,\mu m\,s^{-1}$, and each experiment consisted of a loading and unloading step.

Figure 7 shows three micrographs from a single indentation experiment. They illustrate that, as the depth of indentation is increased, we observe an increasingly large (nearly circular) contact region and an increasing compressive force. At a critical load the sharp optical contrast between contacting fibrils (dark) and non-contacting void space (light) is lost in a region usually, but not always, near the centre of the contact zone, where the fibrils have buckled. With increasing load the buckled region grows in a circular manner, surrounded by an annular region of contacting, unbuckled fibrils. On unloading the converse occurs, but consistent with previous theoretical work (Sharp *et al.* 2004) the buckled region at the same total applied force is larger during unloading than during loading. As we mentioned above, this hysteresis is attributed to the fact that the Euler buckling load is modified significantly due to end-adhesion of the fibrils.

Figure 8 shows results for the effective modulus and the effective work of adhesion as functions of fibril width. These quantities were extracted from the spherical indentation experiments using equations (3.6) and (3.7). Note that there is a systematic decrease in effective elastic modulus with decreasing fibril width $2a$. Compared to flat PDMS, each fibrillar interface has approximately half the contact area ($f = 1/2$). While the aspect ratio of fibrils increases with decreasing a (because h is fixed at $30\,\mu m$), the contact area does not. If the compliance of the fibrillar region were controlled by deformation of fibrils along their axis (as assumed in a conventional Winkler foundation model), one would expect a reduction in effective elastic modulus going from a flat to a fibrillar interface because of reduction in cross-sectional area. However, one would expect no further reduction in modulus with an increase in aspect ratio at constant f. The fact that there is a continued decrease in effective modulus indicates that fibril bending and/or shearing plays an important role in determining the compliance of the interfacial region, even when $\theta = \pi/2$. Note that our theory in equation (3.5) shows that fibril bending makes the effective compliance quite sensitive to the aspect ratio $h/2a$, if the angle between the fibril and substrate deviates at all from 90°.

Figure 8*a* shows a significant difference in stiffness between buckled and unbuckled samples, confirming that buckling does make a more compliant interface. The JKR test produces an effective measure of compliance of the material that characterizes the fibrillar region and the bulk material behind it. Therefore, the compliance of the interfacial region itself is certainly affected more dramatically by change in aspect ratio and by buckling than indicated by these data.

Observe from figure 8*b* that the effective work of adhesion for the fibrillar samples is approximately halved compared to the flat unstructured surface. Indeed, because the dimensions of these fibrils are relatively large (Hui *et al.* 2004), one expects little else for a contact area fraction of $f = 1/2$. However, it is important to note the dramatic reduction in measured work of adhesion for those cases where buckling occurred. From the data in figure 8, we see that these cases yield values of both E^* and W_{ad} that differ significantly from those cases where buckling did not occur.

We compare in Table 2 the experimental and theoretical fibril buckling loads, equations (3.8) and (3.12). Theory and experiment agree very well for the $5\,\mu m$ fibrils and within an order of magnitude for the $10\,\mu m$ fibrils. We have previously observed that experimental buckling loads for the $10\,\mu m$ case are substantially lower than those predicted by theory (Sharp *et al.* 2004). This is not surprising, considering that the aspect ratio in this case is only 3, whereas an aspect ratio of at least 5 is required for beam theory to be accurate.

Table 2. Experimental and theoretical buckling loads (N), for two fibril widths and two indenter speeds.

	Indenter speed $= 1\,\mu m\,s^{-1}$		Indenter speed $= 10\,\mu m\,s^{-1}$	
	$2a = 2w = 5\,\mu m$	$2a = 2w = 10\,\mu m$	$2a = 2w = 5\,\mu m$	$2a = 2w = 10\,\mu m$
Experiment	0.64 ± 0.01	2.72 ± 0.02	0.72 ± 0.01	2.77 ± 0.03
Theory	0.58	6.31	0.614	6.39

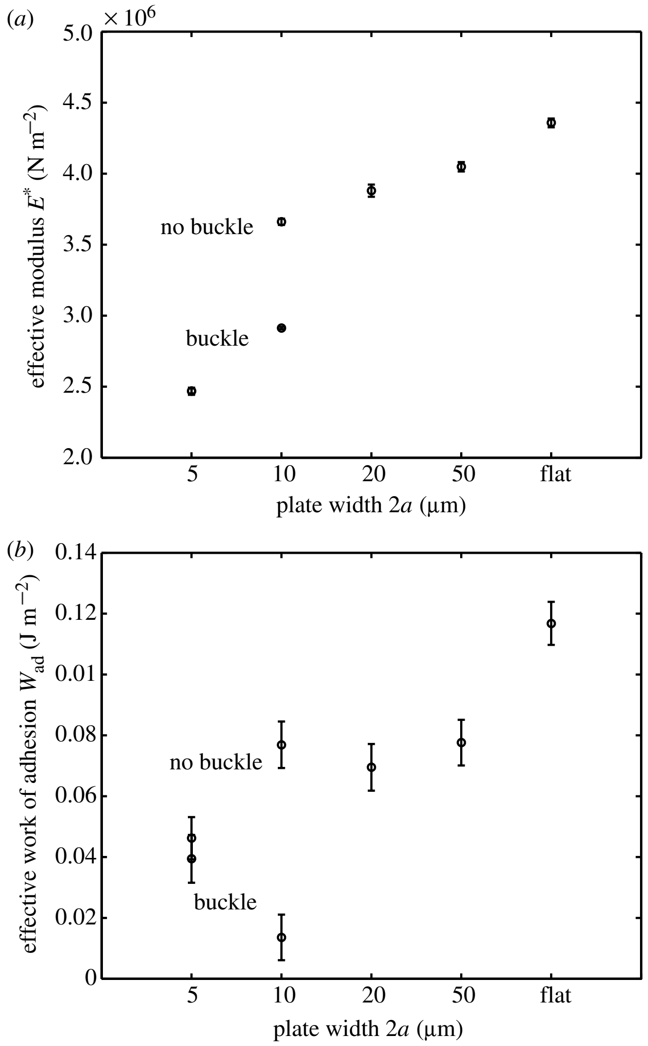

Figure 8. (a) Effective modulus of a plate-like fibrillar PDMS surface as a function of fibril width. Buckling significantly reduces the effective modulus of the material. (b) Effective work of adhesion of a plate-like fibrillar PDMS surface. There is no enhancement of adhesion in these structures, because of their relatively large length scale. However, the data show that buckling is detrimental to adhesion. Each data point is the average of five trials. Error bars show one standard deviation of the variability in the data. The loading rate is $1\,\mu m\,s^{-1}$.

4.2. Lateral collapse

When the critical condition for lateral collapse (equation (3.22)) is just met, only doublets are allowed, as larger groups clumped together require greater bending for outer fibres, which is energetically unfavourable. For sufficiently long fibrils, we observed in experiments that lateral collapse does not necessarily occur in pairs. If one significantly exceeds the critical length, clumps of fibrils with characteristic clump size d tend to stick together. Note that, in spite of this, the minimum energy configuration remains that of all the fibrils pairing into doublets. However, from our observations, it is clear that larger clumps of fibrils are allowed.

One may estimate the characteristic size of the largest allowed clump quite simply by modifying the arguments for doublet formation. Rather than viewing equation (3.22) as a constraint on h, we now identify it as a constraint on w and use it to determine the maximum value of deflection allowed, $w_{\max}$. This value can be interpreted directly as the radius of the clump. Specifically, the maximum clump size will be such that the furthest fibre in the clump is within a radius $w_{\max}$ of the central fibre. This argument neglects the fact that the clumped fibrils will accumulate and take up some space at the centre of the clump radius, so that the actual clump radius $d/2$ will be slightly larger than $w_{\max}$. This fact can be ignored for a small fibril area density f, which is the case for the experimental samples considered in this section.

Figure 9 shows images of post-like PDMS fibrils ($h = 10\,\mu m$, $a = 0.6\,\mu m$) with different separations. As fabricated (figure 9a), we obtain large defect-free areas with fibrils standing separate and protruding from the surface. According to equation (3.22), the fibrils need to be shorter than 4.49, 3.38 and $2.27\,\mu m$, for spacings $2w$ of 2.50, 1.42 and $0.64\,\mu m$, respectively, to avoid any lateral sticking once brought into contact. Thus, although it is possible to fabricate these fibrillar arrays with no lateral sticking over large areas, once they are brought into contact surface forces are sufficient to keep them sticking.

Figures 9b–d show that, although regions of upright fibrils are obtained, when they contact each other they adhere, as predicted. Theory predicts a characteristic clump radius $w_{\max} = 6.2\,\mu m$ for the samples in figure 9. Good agreement is obtained between theory and experiment in that we have not observed clumps larger than this size in any of the samples. Note that smaller clumps are possible, as described above, and are present in the samples. Figure 9e is an image of the fibrillar surface during indentation by a glass sphere. In regions that have not collapsed laterally, there is good contact. However, in regions where lateral collapse is prevalent, many of the fibril ends do not make contact. As will be shown in the companion paper (Hui *et al.* 2004), this has significant deleterious consequences for adhesion.

All the discussion in this section so far has pertained to lateral collapse of fibrils in a single layer. Most morphologies of fibrillar structures in reptiles display

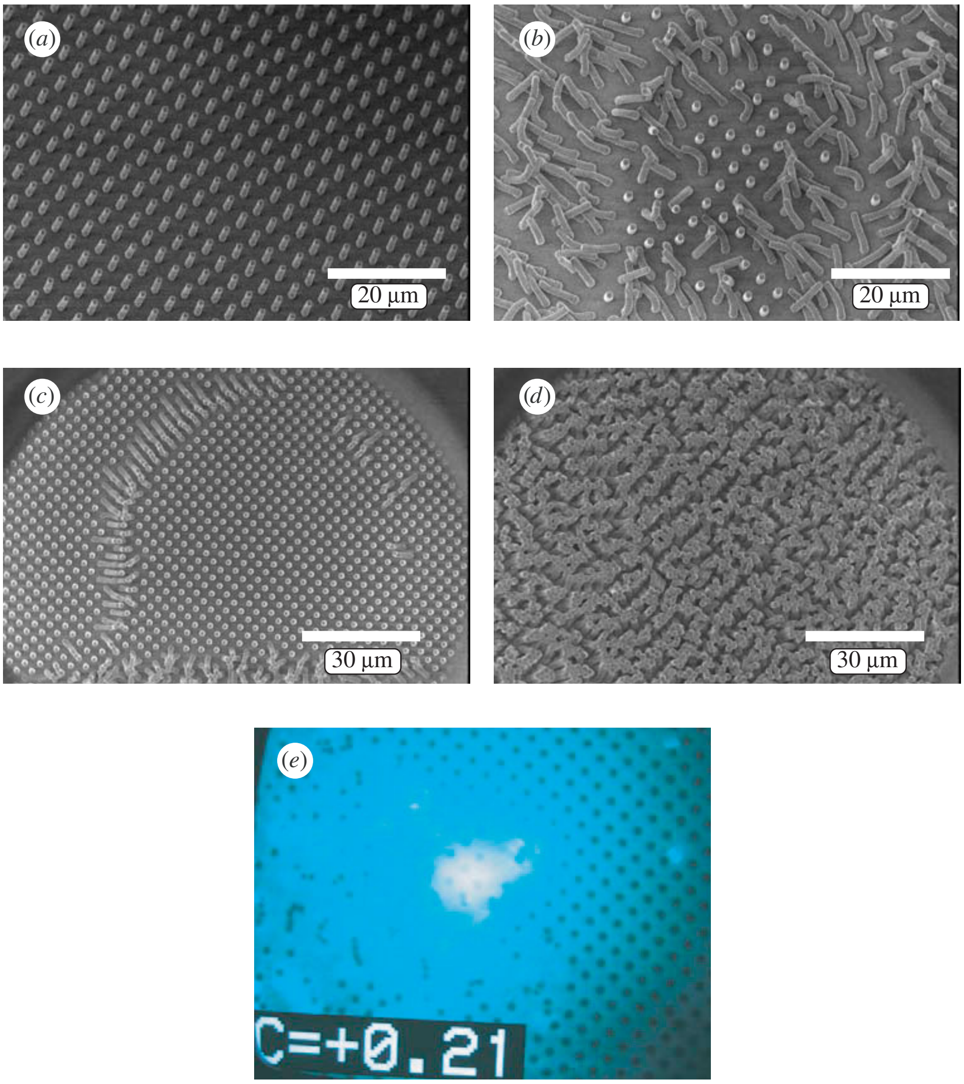

Figure 9. Top view of PDMS fibrils with 1.2 μm diameter, 10 μm length and three different lateral spacings. (*a*) As fabricated, we obtain large defect-free areas. (*b*)–(*d*) When brought together during contact experiments or for other reasons, fibrils adhere to each other laterally: (*b*) $2w = 2.5$ μm; (*c*) $2w = 1.4$ μm; (*d*) $2w = 0.6$ μm. (*e*) Uniform contact by fibril ends is affected deleteriously by their lateral collapse.

a hierarchical structure spanning several levels. Our understanding of lateral sticking suggests that the length scales at which separate fibrils coalesce into bigger bundles in the hierarchy correspond to the critical lengths calculated above in (3.22). In other words, the hierarchical structure is optimized to avoid lateral sticking.

It is interesting to compare our approach to that of Persson (2003*a*), who has also addressed the question of lateral collapse (termed there as 'fibre condensation'). Both approaches are based on balancing the increase in internal energy due to elastic deformation in bending fibrils against its decrease due to released work of adhesion when fibrils come into lateral contact with each other. Persson assumes a mode of deformation in which straight fibres all bend collectively in one direction to form a bundle. In contrast, we treat a mode of deformation observed in our experiments, the basic unit of which is two fibres collapsing by bending towards each other (figure 9). The two treatments result in different predictions for how lateral collapse will scale with materials and geometric parameters. The predictions presented here are in good quantitative agreement with experiments on our model systems (see also Sharp *et al.* 2004).

5. SUMMARY AND CONCLUSIONS

In this first part of two companion papers we have discussed the mechanics and physics of contact through a fibrillar interface. Our focus here is on enhanced compliance bestowed by bending and micro-buckling of fibres and on the limitations imposed by their lateral collapse under the influence of surface energy. We have studied both aspects of contact mechanics by developing simple analyses and by experiments on model materials.

Buckling has been verified experimentally both under uniform and non-uniform (spherical indentation) loading. Our models for the buckling mode of deformation are in good quantitative agreement with experiments on model materials. The spherical indentation experiment has been analysed to extract effective modulus and work of adhesion. The effective elastic modulus of the fibrillar interface is lower than that of a flat control and decreases with increasing fibril aspect ratio. We attribute the decrease in modulus with fibril bending. We also predict and observe experimentally that buckling causes a dramatic reduction in effective modulus. In our samples, however, buckling causes attendant loss of contact between the fibril end and the substrate, hence reducing adhesion.

Lateral collapse of fibrillar structures poses an important design constraint on their fabrication. We have developed a quantitative model for it based on a marginal energy balance between stored elastic and surface energy. Cross-sectional design can play an important role in mitigating lateral collapse for stiffer fibres but we show that it is relatively insignificant only for soft polymeric materials. The predictions of our model are supported by lateral collapse phenomena observed in experiments.

We are grateful to R. G. Bender for the technical assistance provided and to K. G. Sharp for fabricating synthetic fibrillar samples for indentation measurements. We also acknowledge N. Rizzo for gathering all scanning electron microscopy image data on biological and synthetic samples. Finally, we thank D. Hallahan for acquiring biological samples and for helpful discussions regarding the design of synthetic fibrillar systems.

REFERENCES

Arzt, E., Gorb, S. & Spolenak, R. 2003 From micro to nano contacts in biological attachment devices. *Proc. Natl Acad. Sci. USA* **100**, 10 603–10 606.

Autumn, K., Sitti, M., Liang, Y. A., Peattie, A. M., Hansen, W. R., Sponberg, S., Kenny, T. W., Fearing, R., Israelachvili, J. N. & Full, R. J. 2002 Evidence for van der Waals adhesion in gecko setae. *Proc. Natl Acad. Sci. USA* **99**, 12 252–12 256.

Autumn, K., Yiching A., Liang, S., Hsieh, T., Zesch, W., Chan, W. P., Kenny, T. W., Fearing, R. & Full, R. J. 2000 Adhesive force of a single gecko foot-hair. *Nature* **405**, 681–685.

Crandall, S. H., Dahl, N. C. & Lardner, T. J. 1978 *An introduction to the mechanics of solids.* Kogakusha: McGraw-Hill.

Geim, A. K., Dubonos, S. V., Grigorieva, I. V., Novoselov, K. S., Zhukov, A. A. & Shapoval, S. Y. 2003 Microfabricated adhesive mimicking gecko foot-hair. *Nature Materials* **2**, 461–463.

Glassmaker, N. J. 2004 PhD dissertation, Cornell University.

Hui, C. Y., Glassmaker, N. J., Tang, T. & Jagota, A. 2004 Design of biomimetic fibrillar interfaces: 2. Mechanics of enhanced adhesion. *J. R. Soc. Interface* (In the press.) (doi:10.1098/rsif.2004.0005).

Hui, C. Y., Jagota, A., Lin, Y. Y. & Kramer, E. J. 2002 Constraints on microcontact printing imposed by stamp deformation. *Langmuir* **18**, 1394–1407.

Hui, C. Y., Lin, Y. Y., Baney, J. M. & Jagota, A. 2000 The accuracy of the geometric assumptions in the JKR (Johnson–Kendall–Roberts) theory of adhesion. *J. Adhes. Sci. Technol.* **14**, 1297–1319.

Jagota, A. & Bennison, S. J. 2002 Mechanics of adhesion through a fibrillar microstructure. *Integr. Comp. Biol.* **42**, 1140–1145.

Johnson, K. L. 1985 *Contact mechanics.* Cambridge: Cambridge University Press.

Johnson, K. L., Kendall, K. & Roberts, A. D. 1971 Surface energy and the contact of elastic solids. *Proc. R. Soc. Lond.* A **324**, 301–313.

Muskhelishvili, N. I. 1951 *Some basic problems of the theory of elasticity* (transl. from Russian by J. R. M. Radok). Groningen: Nordhoff.

Peressadko A. & Gorb S. 2004 When less is more: experimental evidence for tenacity enhancement by division of contact area. *J. Adhesion* **80**, 247–261.

Persson, B. N. J. 2003*a* On the mechanism of adhesion in biological systems. *J. Chem. Phys.* **118**, 7614–7621.

Persson, B. N. J. 2003*b* The effect of surface roughness on the adhesion of elastic plates with application to biological systems. *J. Chem. Phys.* **119**, 11 437–11 444.

Rischick, D. J., Austin, C. C., Petren, K., Fisher, R. N., Losos, J. B. & Ellers, O. 1996 A comparative analysis of clinging ability among pad-bearing lizards. *Biol. J. Linn. Soc.* **59**, 21–35.

Scherge, M. & Gorb, S. N. 2001 *Biological Micro and Nanotribology: Nature's Solutions.* Berlin: Springer-Verlag.

Sharp, K. G., Blackman, G. S., Glassmaker, N. J., Jagota, A. & Hui, C. Y. 2004 The effect of stamp deformation on the quality of micro-contact printing: theory and experiment. *Langmuir* (In the press.) (doi:10.1021/la036332+).

Timoshenko, S. P. & Gere, J. M. 1961 *Theory of elastic stability.* New York: McGraw-Hill.